Journal of Pharmacokinetics and Pharmacodynamics, Vol. 33, No. 6, December 2006 (© 2006)
DOI: 10.1007/s10928-006-9031-3

Physiologically Based Synthetic Models of Hepatic Disposition

C. Anthony Hunt,[1,2,4] Glen E. P. Ropella,[2] Li Yan,[1] Daniel Y. Hung,[3] and Michael S. Roberts[3]

Received January 23, 2006—Final August 17, 2006—Published online October 19, 2006

Current physiologically based pharmacokinetic (PBPK) models are inductive. We present an additional, different approach that is based on the synthetic rather than the inductive approach to modeling and simulation. It relies on object-oriented programming. A model of the referent system in its experimental context is synthesized by assembling objects that represent components such as molecules, cells, aspects of tissue architecture, catheters, etc. The single pass perfused rat liver has been well described in evaluating hepatic drug pharmacokinetics (PK) and is the system on which we focus. In silico experiments begin with administration of objects representing actual compounds. Data are collected in a manner analogous to that in the referent PK experiments. The synthetic modeling method allows for recognition and representation of discrete event and discrete time processes, as well as heterogeneity in organization, function, and spatial effects. An application is developed for sucrose and antipyrine, administered separately and together. PBPK modeling has made extensive progress in characterizing abstracted PK properties but this has also been its limitation. Now, other important questions and possible extensions emerge. How are these PK properties and the observed behaviors generated? The inherent heuristic limitations of traditional models have hindered getting meaningful, detailed answers to such questions. Synthetic models of the type described here are specifically intended to help answer such questions. Analogous to wet-lab experimental models, they retain their applicability even when broken apart into sub-components. Having and applying this new class of models along with traditional PK modeling methods is expected to increase the productivity of pharmaceutical research at all levels that make use of modeling and simulation.

KEY WORDS: physiologically based; liver; modeling (modelling); simulation; discrete event; agent-based.

[1]The UCSF/UCB Joint Graduate Group in Bioengineering, University of California, Berkeley, CA, USA.
[2]The Department of Biopharmaceutical Sciences, Biosystems Group, University of California, 513 Parnassus Ave., S-926, San Francisco, CA 94143-0446, USA.
[3]School of Medicine, Princess Alexandra Hospital, University of Queensland, Woolloongabba, Queensland, 4102, Australia.
[4]To whom correspondence should be addressed. E-mail: a.hunt@ucsf.edu

ABBREVIATIONS

CV – central vein
ISL(s) – *in silico* liver(s)
N1, N2,... – a set of experiments that explores sinusoidal network arrangement
PBPK – physiologically based pharmacokinetic
PCs – properties and characteristics
PK – pharmacokinetic
PV – portal vein
S1, S2,... – a set of experiments that explores spatial relationships within and between sinusoids
S_A and S_B – two classes of SS
SD – standard deviation
SM(s) – similarity measure(s)
SS(s) – sinusoidal segment(s)

INTRODUCTION

A key goal in developing pharmacokinetic (PK) models is to use simulation to facilitate drug development and clinical pharmacology. PK modeling has undergone considerable evolution in its efforts to achieve this goal. Nonparametric analysis makes no model assumptions about the body but only provides moment data, which may be used to generate PK parameter values. More commonly, data are analyzed assuming the body may be described as an abstract series of compartments or, in physiologically based pharmacokinetics (PBPK), by representing organs as compartments connected to represent a vascular system (1,2). These and related model types are by nature *inductive*: they are a cognitive reduction of the biology to describe PK data, using representations of the hypothesized essential determinants governing the measured phenomena. Almost all of these models rely on systems of equations[1] (typically differential equations) and/or probabilistic networks to represent or describe essential features of PK data.

In this report, we introduce and demonstrate an additional approach (as distinct from alternative) to PBPK modeling—one that is based on the synthetic, rather than the inductive method. A discretized analogue of the system that generated the data is constructed from *independent* components. It relies on object-oriented programming, and is constructed using software objects that are representations of body components. Design and

[1] Inductive models can take any form. Equations fit to data are just one example.

construction is guided by intended model uses, the problem being solved, and model requirements, as well as the available data. Different objects represent biological components that vary in size, type, and function. Some represent molecules, others represent cells, and still others represent aspects of tissue architecture, etc. The components are composed within a software environment that includes a representation of the experimental PK context (including the experimenters), and facilitates a cycle of creating, verifying, and changing models. Experiments are then conducted on the *in silico* analogue in the same ways that wet-lab PK experiments are conducted. In this way, the analogue system reflects the entire experimental system of interest. Simulated PK data are collected and compared to referent PK data, when the latter are available. An acceptable degree of similarity is taken as evidence supporting the hypothesis that the assembled components have generative properties that mimic those of the corresponding biological components: they are biomimetic. They exhibit their own phenotypic attributes. They can adapt easily to new situations, such as becoming a components of whole-body models. The envisioned analogues are not alternatives to traditional PK models: the two classes of models serve different purposes and so can be synergistic.

Recognizing that the first goal in PK modeling has been to provide descriptions of the organ (3), we have limited this report to representing aspects of the rat liver, as viewed from the perspective of sucrose administered together with antipyrine. This approach is consistent with the notion that "an overall objective of physiological modeling is to simulate the complete system through a fundamental study of its component parts" (1).

PHYSIOLOGICALLY BASED MODELING

The Vision

PBPK models recognize anatomical and physiological realities, and attempt to account for the role of differential distribution within and between organs as well as their varying blood flows (4). The expected heuristic value of PBPK modeling in research, drug development and regulatory science, and toxicological risk assessment is evident in the variety of envisioned model uses discussed in several recent reviews (4–6). Several desired and anticipated advantages of PBPK models have been cited (4, 5), but not yet realized, of which the following are just a few. It should be straightforward to reuse a parameterized PBPK model to explore the expected behaviors of different compounds. Models should be capable of reflecting whatever physiological detail is relevant to the problem. Updating needs to be facile. One should be able to replace low-resolution

components with more detailed ones that will enable the simulation of mechanistically based pharmacodynamics (4,7) or to account for changes in rate-limiting steps or relevant heterogeneity within tissues and cells (8,9). Realization of these uses is expected to allow researchers to answer important questions such as: can we predict the PK behavior of a new, unstudied compound by studying synthetic models validated against other compounds with different PK behavior? Can we provide increasingly confident explanations of events within target sites, and can we adjust those events to take into account patient specific knowledge?

Inductive and Synthetic Methods

The inductive method for creating models dominates the PK literature. Inductive models, by definition, abstract away the very detail required by heuristic PBPK modeling. This has lead to top-down attempts to graft details onto the highly abstract inductive models. Augmenting PBPK modeling with the more flexible synthetic method provides a middle-out strategy with two primary benefits: (1) a deep physiological model–to–referent mapping and (2) access to unpredictable systemic phenomena in the model (e.g., those that may result from nonlinearities). Inductive methods, especially those dependent on continuum mathematics like ordinary differential equations, often rely on assumptions like linearity for their mathematical basis. Hence, any model developed with induction exhibits only the behaviors present, *a priori*, in the model *family* used for induction. Synthetic PBPK modeling involves using independent components to build a functioning analogue of the *mechanisms* (form and function; component interactions) of which an inductive PBPK model is an abstraction. Being composed of separate sub-models (10–14), synthetic models provide more flexibility in representation and underlying assumptions[2]. We posit that this flexibility is critical to the satisfaction of the core requirements of PBPK modeling and thereby achieving the vision.

APPLYING MODELING PRINCIPLES

Models of Hepatic Elimination

How will changes in hepatic details alter the hepatic disposition of two compounds administered simultaneously? Traditionally, answers have been obtained using appropriately designed *in vitro* and *in vivo* experiments. Sometimes they are not enough: the appropriate experiment

[2]We expand our ideas of *inductive* and *synthetic* modeling in Supplementary Material.

can be impossible, too challenging, too costly, take too long to set up and complete, or the researcher may be unable to uncover the precise intrahepatic events. It would be desirable to be able to conduct experiments *in silico* that would provide useful answers to questions, coupled with a useful measure of uncertainty. The following three questions are examples of what can be addressed using *in silico* experimentation on synthetic models:

1. How might zonal differences in metabolizing enzymes influence the hepatic elimination and metabolic profiles of compounds *A* and *B* when they are co-administered relative to being administered separately, especially when one pathway for metabolism is saturated?
2. How might hepatic elimination respond to a pharmacological or an inflammation-induced reduction in sinusoid diameters, recognizing that vasoconstriction is often associated with ischemia-reperfusion injury?
3. Can a significant difference in the ratio of metabolizing enzymes to various transporter activities, within or between cells (in PK terms, the relative contributions of intrinsic clearance and hepatic permeability clearance) account for some of the interindividual differences in the dose dependent hepatic clearance of some drug?

In this report, we provide a cornerstone for a solid foundation that can be built upon and extended to produce models that can answer such questions. It is envisioned that the ISL (*in silico* liver) will have many properties and behaviors that partially overlap those of the current inductive models of hepatic elimination[3]. They will also be capable of exhibiting properties and behaviors that are not achievable by those inductive models. During early development of a new class of models, it is best to have trusted, successfully used models that, for overlapping behaviors, can serve as standards, against which to contrast members of the new class of models. A primary reason for focusing on the liver and hepatic elimination in this report is that the already existing rich literature provides multiple options for cross-model validity.

Model Usage

The hepatic outflow profile of a compound is a phenotypic attribute. The greater the similarity between the measured behaviors of an ISL and known attributes of a liver, the more useful that ISL will become as a

[3]Discussions of the variety of hepatic models used in PK can be found in Refs. (8) and (15).

research tool and as an expression of the coalesced, relevant knowledge of the liver. In this report, we focus on hepatic outflow profiles of sucrose and a co-administered drug, antipyrine. To simulate the complete system through a fundamental study of its component parts (1), this research will produce increasing overlap between ISL behaviors, properties, and characteristics, and measures of hepatic phenotypic attributes.

The long-term goal of this research is to produce increasing overlap between ISL behaviors, properties, and characteristics, and measures of hepatic phenotypic attributes. Achieving that goal depends on demonstrating models that achieve at least 10 capabilities:

1. The models are capable of accurately representing *intrahepatic events*.
2. There is clear *physiological mapping* between referent and model components because ISL observables are designed to be consistent with those of the referent liver.
3. When dosed with a simulated compound, the ISL generates outflow data that are, to a domain expert (in a type of *Turing test*), experimentally indistinguishable from the referent wet-lab data; this requires that the ISL and its framework must be suitable for experimentation.
4. To enable the above capabilities and support 6–9 below, the ISL and its framework must use *discrete interactions*.
5. The ISL must be *transparent*: the details of the simulation, as it progresses, need to be visualizable and measurable.
6. The components *articulate*: it must be easy to join, disconnect, and replace ISL components.
7. The ISL components can be easily *reconfigured* to represent different histological, physiological, or experimental conditions.
8. It must be relatively simple to change usage and assumptions, or increase or decrease detail in order to meet the particular needs of an experiment, without requiring significant re-engineering of the model.
9. The ISL must be reusable for simulating the disposition, clearance, and metabolic properties of *multiple compounds* in the same experiment, not just one each in separate experiments.
10. The ISL must be constructed so that it can eventually function as an organ component within a larger, synthetic, physiologically based, whole organism model.

Specification of an *In Silico* Liver

To enable achieving the 10 capabilities, we discretize hepatic anatomy and physiology so that important aspects of structure are mapped to directed graph structures. We specify only the minimum number of hepatic features needed to generate the required output and exhibit the specified features. Features and functions that are currently not needed are not explicitly specified. Instead, they are conflated with other ISL components. When one of these features or functions is needed, it can be brought back into focus and assigned to newly added components without requiring significant re-engineering of the components already present.

The hepatic parenchyma of the rat is organized as several polyhedral primary units—lobules—integrated into larger secondary units (16). We assume that secondary unit functions are similar throughout a normal liver, and that each has similar incoming and outgoing fluid flows. By making that assumption, we can collapse the graph that would be needed to represent the entire liver into a directed graph of parallel single nodes, each representing a secondary unit. The integration of a dozen or so lobules into a secondary unit results from a common drainage by its branches to form a central venular tree, and from the arrangement of portal tracts and vascular septa that form a continuous vascular surface over the entire unit. Because of their structure, secondary units can be accurately represented as small networks of primary lobules. If we assume that all lobules in a secondary unit are similar in form and function, then we can collapse the secondary unit graph structure into a single node (a typical lobule) having one incoming and outgoing edge. The organization of this typical lobule is pictured in Fig. 1.

The arterial and portal vein (PV) blood supply for one lobule feeds into several dozen sinusoids that merge in stages to only a small fraction of their original number as they feed into the lobule's outgoing central vein (CV). Those flow paths can also be represented by an interconnected directed graph. Objects representing sinusoidal spaces and function can be placed at the graph nodes. Within the ISL, those objects are software agents[4] called Sinusoidal Segments (SSs). Their design is discussed below and illustrated in Fig. 2. Hepatic intralobular heterogeneity and zonation are well documented (19,20). Hepatic cells, including hepatocytes, can exhibit location-specific properties within lobules (16,21), including location-dependent expression of drug metabolizing enzymes (8) and transporters. Different sinusoids can experience different flows (22) and have

[4]Technically, an agent is a software object with the ability to interact with its environment and schedule its own actions. The work of Peirce *et al.* (17) and An (18) are examples of successful application of agent-based models to complex biological systems.

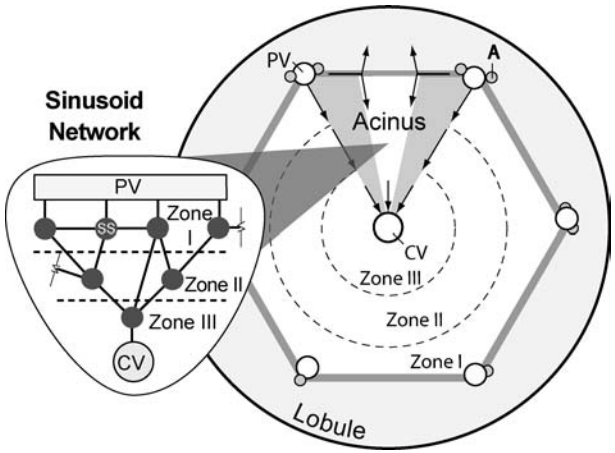

Fig. 1. A schematic of an idealized cross-section of a hepatic lobule showing half an acinus and the direction of flow between the terminal portal vein tract (PV), and the central hepatic vein (CV). Expansion: within the ISL, flow paths are represented by an interconnected, three zone, directed graph. Data from the literature are used to constrain the graph size and structure. A portion of the graph connects *in silico* PV outlets to the CV is shown. SS: sinusoidal segment.

different surface-to-volume ratios. As needed, such heterogeneity can be easily represented by differences within and between SSs. Interconnections between sinusoids are frequent in the periportal region, but are rare near the CV. Teutsch *et al*. (16) subdivides the lobule interior into six concentric zones to quantify the enzymatic gradients between PV and CV. When attention is limited just to drug outflow profiles, one or two zones may be adequate. However, we want to be able to explore the consequences of such zonation. For that, having three zones (I, II, and III in Fig. 1) is adequate to start. When considering sucrose and antipyrine outflow data, bile can be ignored. When needed, an additional outgoing edge and SS detail can be added in to represent bile flow.

To avoid confusion hereafter and clearly distinguish *in silico* components from corresponding *in vitro* and *in vivo* hepatic structures such as a lobule, spaces such as fenestrations, objects such as an hepatocyte or a compound, or a process such as metabolism or partition, we use SMALL CAPS when referring to the *in silico* counterparts.

Lobule Structure

We assume that there are many arrangements of lobule flow paths that will give similar outflow profiles for a given compound. We want to identify the *in silico* counterpart of that set and sample from it, thereby

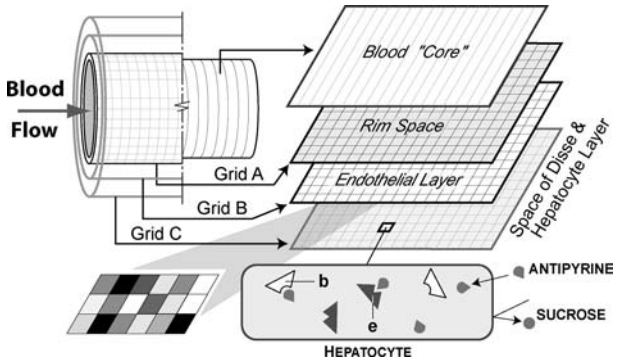

Fig. 2. A schematic of a sinusoidal segment (SS): one SS occupies each node specified by a directed graph (Fig. 6). Grids represent spaces and can contain objects representing the functions associated with sinusoids. Objects representing ANTIPYRINE and SUCROSE enter and exit via the Core and Rim, and can access any of the other three spaces. Grid locations can have properties and axioms that govern their interaction with mobile objects and their neighbors. The potential for heterogeneous properties within different spaces is illustrated by the expanded portion of Grid B having different shadings. Objects functioning as containers (for other objects) are used to represent cells, and can be assigned to any grid location; a HEPATOCYTE container is shown; objects representing all needed intracellular components can be placed within those containers. Only two types of INTRACELLULAR binders recognize ANTIPYRINE; those that only bind (b) and those that also metabolize (e). A CELL container will not allow SUCROSE to enter.

parameterizing a specific LOBULE. For practical purposes, we need to circumscribe that space. We do that by applying several physiologically supported constraints. The resulting set of LOBULE architectures is large but manageable. During parameterization, if a given structure fails to generate acceptable outflow profiles, additional components are added or removed and parameterized until outflow profile requirements are met. Adding or removing a component, such as a graph node or edge, has no impact on the function of any other component. Progress from a heuristic to a predictive device is made in this fashion.

The three-zone structure requires that each zone contain at least one node. In a later section, we discuss limiting the number of zones. Sinusoidal segments (Fig. 2) are placed at each graph node. We specify that the shortest path (from PV to CV) will pass through no more than one node per zone; the shortest path allowed contains a single node. The expanded section in Fig. 1 illustrates a portion of a network structure that connects PV outlets to nodes in Zone I, from these nodes to nodes in Zones II and III, and finally from there to the CV. Graph structure is specified by two parameters: the number of nodes in each zone and the number of edges between nodes. A full list of parameters is provided in the Appendix.

The graph edge that connects one node to another specifies a "flow path." These paths have zero length and contain no objects.

We allow for a specified number of cross-connections between nodes within Zones I and II, but not within Zone III. The number of such intra-zone connections is a parameter. However, the assignment of connections is randomized for each run to simulate intrahepatic variability. There are also a specified number of inter-zone connections. Their assignment too is randomized for each run. When searching the circumscribed LOBULE space for suitable graph structures, the experimenter, keeping in mind the approximate proportion of the total lobule volume found in each zone, assigns an initial set of parameter values; runs the experiment; checks the results; and then, if improved results are needed, modifies one or more parameter values. When a similarity measure is available, this process can be automated. In this way, the circumscribed parameter space is sampled to find an acceptable region. For a given LOBULE parameterization, the number of nodes per zone is specified, as are the numbers of intra- and inter-zone edges. In a given run, if a node is left with no outlet, then it is connected directly to the CV.

SINUSOIDAL SEGMENT Design

We have studied outflow properties using several sinusoidal segment designs, and report here on one. Simpler designs generate behaviors that fail to meet either a specification or our similarity measure criterion. A SS is modeled as a tube-like space with a rim surrounded by two additional spaces. The tube and rim represent the central sinusoidal space and its immediate borders. The tube contains a fine-grained abstract "Core" space that represents blood. Grid A, the Rim, represents sinusoid edges near endothelial cells. A fine-grained space (Grid B) is wrapped around Grid A to represent the endothelial layer. Another space (Grid C) is wrapped around Grid B to collectively represent the Space of Dissé and hepatocytes. Because we are building a normalized model, there is no direct coupling between locations within a grid and real measures such as actual hepatocyte volume or fenestrae size. Additional spaces can be added when additional functionality is needed, and any of the current spaces can be turned off (removed) if they are not needed, without interruption of remaining functionality.

The relative grid dimensions and number of locations per grid (both of which are flexible) determine the resolution. The properties of a grid location can be homogeneous or heterogeneous depending on the specific requirements and the experimental data being considered. Heterogeneous properties are illustrated by the different Grid B shades in Fig. 2. Objects

can be assigned to any grid location. Currently, unassigned locations in Grid B represent intracellular gaps and fenestrae for object sieving into the simulated Space of Dissé. The remainder of Grid B is assigned to ENDOTHELIAL CELLS. Kupffer and/or stellate cell behaviors can be added as they are needed. A large fraction of Grid C space is assigned to HEPATOCYTES.

To further account for sinusoidal heterogeneity, including differences in transit time and flow (23), topographic arrangement (24), and the different surface-to-volume ratios within zones (19,22), we defined two SS classes: $\boldsymbol{S}_A$ and $\boldsymbol{S}_B$. From preliminary efforts to simulate sucrose outflow profiles using earlier models we learned that a variety of SS lengths would be needed. Relative to $\boldsymbol{S}_B$, the $\boldsymbol{S}_A$ have shorter path lengths and smaller surface-to-volume ratios. The circumference of both SS classes is specified by a random draw from a uniform distribution having maximum and minimum values. To reflect the observed relative range of real sinusoid path lengths, SS length is given by a random draw from a modified gamma distribution having a mean and variance as specified in the Appendix. The minimum length accepted is two grid spaces for $\boldsymbol{S}_A$ and ten for $\boldsymbol{S}_B$.

Movement of COMPOUNDS In Silico

A mobile object serves as a passive representative of a compound as it moves through the LOBULE. The process represents molecules moving through sinusoids. The relative tendency of a COMPOUND to move forward within the SS determines an effective flow pressure, and that is governed by a parameter called *Turbo*. If there is no flow pressure (*Turbo* = 0), then COMPOUND movement is specified by a simple random walk. Increasing *Turbo* biases the random walk in the CV direction. The dosage function is a modified gamma function, rather than an impulse. This is in part to account for the effects of catheters and large vessels as detailed in Refs. (9) and (25), and is based on values used by Hung *et al.* (2).

The behavior of a COMPOUND is dictated by axioms[5]. Axioms specify relationships between COMPOUND properties, location, and proximity to other objects and agents. The axioms can be structured to recognize and take into account relative compound-specific physicochemical properties (26,27). A COMPOUND that arrives at a grid location assigned to a cell may, with a specified probability, undergo simulated partitioning and

[5]We use *axiom* to emphasize that computer programs are mathematical, formal systems and the initial mechanistic premises in these simulations are analogous to axioms in formal systems.

enter that CELL, stay put, or move to a new location. The CELL disallows SUCROSE, but not ANTIPYRINE, to partition because it "sees" that an assigned SUCROSE property indicates that it cannot partition across CELL membranes. The analogue of a compound that can partition will enter CELLS. Within a CELL, the object can become subject to additional axioms reflecting the intracellular environment (26–29). Grid B represents an endothelial boundary rather than a navigable space. Within it, a parameter controls the size and prevalence of FENESTRATIONS: 5% is randomly assigned to FENESTRAE; the remaining 95% is assigned to CELLS. Similarly, within Grid C a parameter controls the relative density of HEPATOCYTES.

The following is a description of how SUCROSE and ANTIPYRINE navigate the network. Each SS outlet is connected to n receiving SS targets. An object will exit one of the n outlets at random. The probability of exit via a chosen outlet is a function of n, the available number of SS outlets, a_i, the inlet area, described below, of each SS ($i = 1, \ldots, n$), and c_i, the "concentration" of other solute objects just inside the target SS inlet. If the object does not exit, then a new outlet is selected from those remaining. If the SS cannot find a place for the COMPOUND (e.g., as a consequence of crowding, as when "concentrations" are high) then the process is repeated up to 10 times. The determinant for whether a SS can find a place in an output node is the estimate of the density of COMPOUND at the entrance of the SS. That density is estimated by the formula for the area of a circle where the radius is derived from the circumference ($r = C/2\pi$); C is the width of Grid A when laid flat. Flow and concentration come about, in part, due to this density calculation. If the simulated concentration is high at any part of the SS, flow out of that area will be increased, resulting from the CONCENTRATION gradient and PRESSURE (more objects trying to move creates a flow effect). Flow is also partly synthesized through adjustment of the *Turbo* and the *coreFlowRate* parameters.

Both COMPOUNDS can enter a SS at either the Core or the Rim. Thereafter, until each is collected at the CV they have several stochastic options, the aggregate properties of which are determined using Monte Carlo techniques. In the Rim or Core a COMPOUND can move within that space, jump from one space to the other, or exit the SS. When the COMPOUND jumps from Rim into Grid B, it can move within the space, or jump back to the Rim or on to Grid C. When it encounters a CELL, SUCROSE moves on. SUCROSE can move within the EXTRACELLULAR portion of Grid C or jump back to Grid B. After it exits a SS in Zone 3, it enters the CV; its passage through the CV is recorded (corresponding to being collected in the fraction collector).

The only subcellular functions needed to represent low clearance antipyrine are binding and metabolism. All cellular components that bind or metabolize antipyrine are conflated into and represented by binding objects placed inside the containers representing CELLS. Metabolism is handled as a special case of binding: enzyme objects bind ANTIPYRINE for some amount of time before either releasing or METABOLIZING it. Binding objects are assigned randomly to all CELLS. Enzyme objects are assigned randomly to HEPATOCYTES. Assignments are randomly drawn from a uniform distribution having a specified minimum and maximum. A binding parameter specifies the number of simulation cycles that ANTIPYRINE is bound. Enzyme objects are programmed to recognize substrates. They use an additional parameter, the probability of being metabolized.

ANTIPYRINE moves within a SS and LOBULE as does SUCROSE, but using its own parameter values. When ANTIPYRINE encounters a CELL within Grids B or C it may partition into the CELL. Once inside it can move about, exit, bind or not bind, and possibly be METABOLIZED. For the simulations that follow, all binding objects within a HEPATOCYTE also METABOLIZE. The probability of an ANTIPYRINE object being METABOLIZED is controlled by a parameter. Once METABOLIZED, that ANTIPYRINE is destroyed (unless we wish to track metabolites).

The means for generating and managing all of the above components and capabilities are organized within a framework, (diagrammed in Fig. 3), and managed in part by an Experiment Agent that serves a role similar to that of a researcher conducting and recording the results of wet-lab experiments. Additional details are provided in the Supplementary Material.

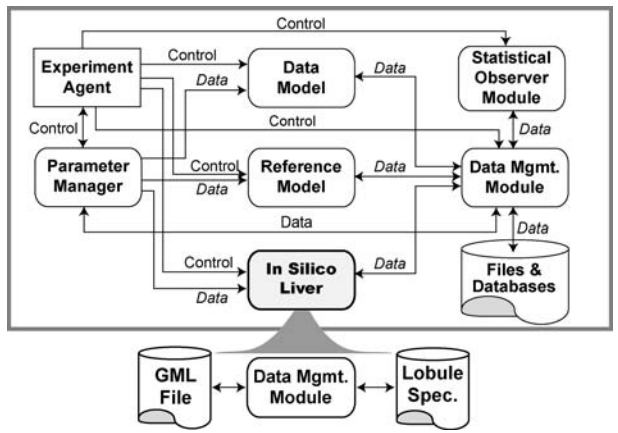

Fig. 3. Framework of the *In Silico* Liver (ISL) showing key components.

The Stochastic Nature of *In Silico* Outflow Profiles

The typical rat liver outflow profile is an account of on the order of 10^{15} or more drug molecules percolating through hundreds of lobules. The typical *in silico* dose for *one* run with one LOBULE uses on the order of 5,000 objects, each representing a number ($\geqslant 1$) of molecules. An outflow profile for such a small number of objects is noisy and is inadequate to represent a PK profile. At times following the outflow peak, it is increasingly possible to encounter an interval during which no objects are collected. A second independent run with that same LOBULE, parameter settings, and dose will produce a similar but uniquely different outflow profile. That is because a single experiment involves thousands of probabilistic events. For each independent run, the seed for the random number generator is changed, altering the specifics for all stochastic parameters. Several stochastic parameters control the ISL organizational and spatial architecture, specifically: the organization of the directed graph, assignment of SS type to each directed graph node, the dimensions of the SS spaces, and how the edges are used to connect SSs. Together, for each run, they provide a unique, individual version of the LOBULE where the relative differences are analogous to the unique relative differences between lobules in the same liver. Differences between runs also simulate some of the uncertainty that is built into the model. The variance across runs in the outflow fraction within a given time interval is neither constant nor deterministic. One ISL experiment combines the results from 10 to 50 independent runs of the same LOBULE.

To reduce outflow profile noise, we use a 70-point smoothing window. The resulting outflow profile (Fig. 4 is an example) is sufficiently smooth for comparison with other profiles. An experimental result comprising 4–7 LOBULE runs[6] is analogous to results one might obtain if one could conduct a perfusion experiment on one hepatic lobule. Assuming the lobules within a normal liver are similar, the sum of the results from 10 to 50 runs can be used to represent the outflow profile of one ISL.

Similarity Measure

When are two outflow profiles sufficiently similar to be considered experimentally indistinguishable? The answer specifies when an *in situ* and an ISL outflow profile are sufficiently similar to be experimentally indistinguishable. For this study we decided that if most of the values of an

[6]The coefficients of variation as a function of time for six repeated *in silico* experiments from Ref. (2) were calculated. The values were higher at earlier and later times. Between 2 and 80 s values ranged from 1.2% to 54.4%, averaging 16.1%.

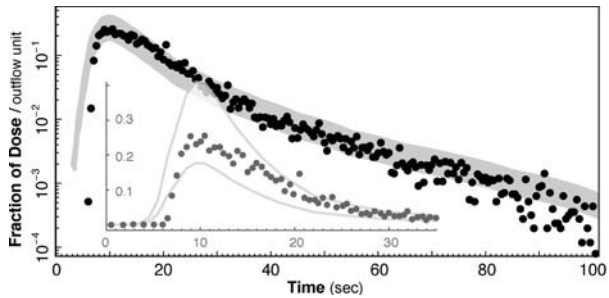

Fig. 4. Semilog and scatter plots show the fraction of dose per outflow unit (per ml for the referent) as a function of time (1 unit = 1 s) after dosing. The dose contained equal amounts of SUCROSE and ANTIPYRINE; only SUCROSE data are shown. The gray band spans the range for the mean ± 1 standard deviation for each of six sucrose outflow profiles from the livers of six matched rats (2). The ISL parameterizations are provided in the Appendix. The data points are smoothed, pooled results for 48 independent runs of the same ISL. Although each independent run uses the same parameter settings (number of nodes per zone, number of edges within and between zones, SS type, etc.) their assignments are randomized; as a result, the actual structure of the LOBULE is different for each of the 48 runs (e.g., see Fig. 6).

ISL outflow profile are within one standard deviation (SD) of mean values obtained from six repeated sucrose experiments, then the ISL data can be considered "experimentally indistinguishable" from that referent data.

For simplicity, we assume that the coefficients of variation of repeat observations within different regions of referent outflow profiles are the same. In that way, we can use a similarity measure (SM) that is a simple, constant proportion interval. Specify a distance, d as the basis for a match. For each observation in reference profile P, create a lower, P^{l}, and an upper, P^{u}, bound by multiplying that observation by $(1-d)$ and $(1+d)$, respectively. The two curves P^{l} and P^{u} are the lower and upper bounds of a band around P. The ISL outflow profile is deemed similar to reference outflow profile if, for example, 90% or more of the second profile stays within the band. In this study d is the standard deviation of the relative differences between each of six replicate sucrose experiments and the mean observations for that collection interval, pooled over all collection intervals. The data are from Ref. (2).

The SM score is the fraction of observations of the candidate time series (typically $\geqslant$100 observations) that fall within the one SD envelope. Because the variability within any ISL run is large, it is unlikely, even for one of the better matches, to have a SM score $\geqslant$0.97. For these studies, 0.8 is the lower limit of acceptable values. A value $\geqslant$0.9 is a quite reasonable match. For some future PBPK models more sophisticated SMs may be needed (as discussed in Refs. (30) and (31)).

RESULTS

In Silico ISL Outflow Profiles

In the referent wet-lab experiments, sucrose and antipyrine were co-administered. In the *in silico* experiments that follow, SUCROSE and ANTIPYRINE were both co-administered and administered separately. Because ANTIPYRINE crosses into CELLS, whereas SUCROSE cannot, the outflow profile for SUCROSE is much more sensitive to SS geometry than is the profile for ANTIPYRINE, and that is a reason that it has been traditionally used as an extravascular marker (32–34). Consequently, parameterizations were done as follows. Lobule and SS structure were first parameterized focusing on just on wet-lab sucrose profiles. Once acceptable SM values were achieved, we held those values reasonably constant and then focused on adjusting the additional parameter values that influenced only ANTIPYRINE. Antipyrine, rather than a more lipophilic, higher clearance drug was selected for assessing feasibility because its disposition properties are similar to those of sucrose. Several iterations of that procedure were needed to obtain acceptable SM values for both COMPOUNDS alone and administered together. Because of the key role of wet-lab sucrose data in determining the *in silico* LOBULE structure, the sections that follow focus mostly on SUCROSE.

An acceptable match for a referent, aggregate sucrose outflow profile is shown in Fig. 4. For 200 observations the SM score was 0.906. The complete set of parameter values, with explanations, is provided in the Appendix. These results demonstrate that ISLs can exhibit five of the targeted capabilities: (1) intrahepatic events are represented; (2) the mapping between ISL and referent physiology is clear; (3) results are experimentally indistinguishable: the "Turing test" was passed; (4) discrete interactions are used; and (5) the transparency in generative components is evident.

The LOBULE structure in Fig. 4 is complicated: 53 nodes, 65 edges, and two types of SS. Is all of that detail needed? It depends on the stated objectives. For small numbers of nodes and edges the frequency distribution of available path lengths and intra-LOBULE residence times is no longer smooth. Clusters form easily within the graph structure, and this causes bumps to appear in the outflow profiles (data not shown). These bumps are smoothed out by having a sufficient variety of path and residence time options.

The profile change induced by a modest change in one parameter can be reasonably compensated for by adjustments in several of the other parameters. However, the relationships that produce the compensations are highly nonlinear. As an illustration, to increase throughput for sucrose

one can: increase circumference of SSs; shorten the SSs; remove cycles from the graph; add more inter-zone edges; remove intra-zone edges; or increase the parameter *Turbo*. Overall, the parameters have overlapping influences and the map between the parameters, their values, and the observables is nonlinear, as would be the case if the analogous properties in the actual liver were modified, were it possible to make such modifications.

For the data in Fig. 4, the ISL parameters were tuned to generate a profile that fit reasonably well within the ±1SD band. The parameters may also be tuned so that ISL output provides an acceptable match to an individual sucrose profile (e.g., one of the six from Ref. (2)). An example is presented in Fig. 5A. The parameter values are listed in the Appendix (Table A2); the SM score was 0.93. The SUCROSE input function, representing the catheter effects in the *in silico* perfused liver system, is shown in Fig. 5B. To obtain that curve all of the SSs were effectively disconnected so that all of the SUCROSE that would have entered the 30 Zone 1 SSs moves directly to the CV where it is collected and measured.

There is one automatically generated graph structure for each ISL run. The graphs corresponding to four of the runs in Fig. 4 are shown in Fig. 6. The graphs were generated using Tulip (www.tulip-software.org/). This graph visualization style shows every node and every edge in a 2D layout for easy visual examination.

There is a direct relationship between the size of the graph, the dose, and the number of runs needed to meet the experimental objectives.

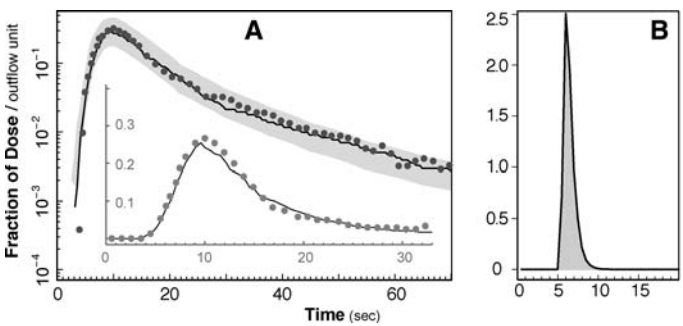

Fig. 5. (A) Semilog and scatter plots show a SUCROSE outflow profile, as in Fig. 4. The ISL parameters have been tuned in the absence of ANTIPYRINE to match a specific sucrose data set: the solid line-segments connect the sucrose data from one rat liver (fraction of dose/ml; from Ref. (2)). The gray band is the same as in Fig. 4. Dark gray circles: SUCROSE outflow values using the tuned parameter set in the Appendix, Table A2. (B) The SUCROSE input function for (A) and for Figs. 4 and 7. The input function simulates the catheter effects, as discussed in the text. The curve was obtained by disconnecting all SSs so that the dose moves directly from PV to CV.

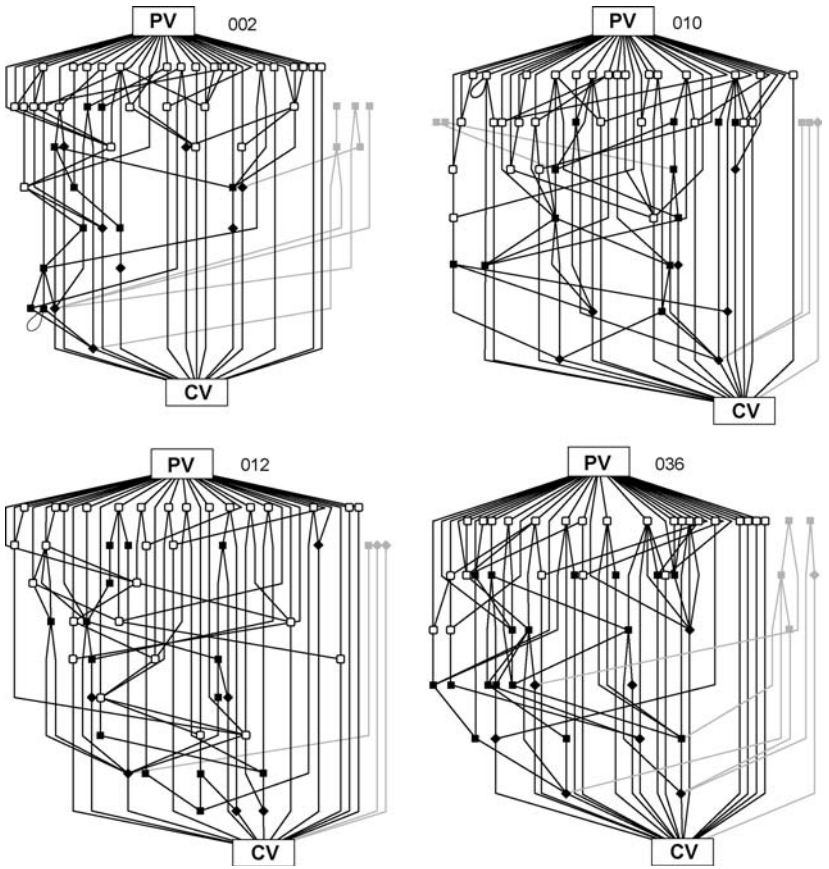

Fig. 6. Graph structures for four of the 48 runs in Fig. 4; the graph generated for run numbers 002, 010, 012, and 036 were selected at random. Graph layout is not organized by zone. All Zone 1 nodes are unfilled, rounded-corner squares; they have one edge connecting them to the PV, and can be connected to other SSs in Zone 1 as well as to other zones. Zone 3 and Zone 2 nodes that are directly connected to the CV are shown as black diamonds. All other Zone 2 nodes are shown as black squares. By chance, an edge exiting one node in both 002 and 010 connects back to that same node; those edges are shown as loops. By chance, the nodes and edges in light gray were not assigned an incoming edge. If, after all 65 edges have been assigned, there is still one or more Zone I or II SS with no outgoing edge, then the SS will be connected directly to CV.

As the dose is metered into the Zone 1 nodes (by the Fig. 5B dosing function), there needs to be sufficient space and available grid locations into which the SUCROSE can move; otherwise, it cannot be metered out as required. In addition, SUCROSE at the leading end of a Zone 1 node needs to get out of the way in order to make room for incoming dose. The larger

the dose, the larger the sum of entry spaces needs to be. For the data in Figs. 4 and 5, that area is determined by SS circumference (Grid A width) and number of nodes in Zone 1. For the simulation in Fig. 4, if dose and nodes are reduced by 50% and the number of runs is doubled, then the results will be the same but total run time is longer; so, there is a trade-off between total run time and model size. Further reductions may not result in equivalent simulations, however. That is because graph interconnectedness can be compromised when there are not enough options.

The results in Fig. 7 show the outflow profile of ANTIPYRINE given alone and in combination with SUCROSE for the same parameterizations as in Fig. 4. It is evident that the ISL and wet-lab profiles are similar. The additional ANTIPYRINE-specific parameter values are listed in the Appendix. With these results, we have demonstrated capability 9 (capable of representing PK properties of *multiple compounds*).

Influences of Parameterization Changes

To demonstrate the sensitivity (or lack thereof) of results to changes in ISL structure or parameterization, we report results from two sets of experiments in which the ISL was dosed with an equal combination of ANTIPYRINE and SUCROSE given together as in the original wet-lab experiments. They were designed to explore the ease with which model features could be changed along with the consequences of those changes, and thereby demonstrate capabilities 6 (easy to join, disconnect, and replace

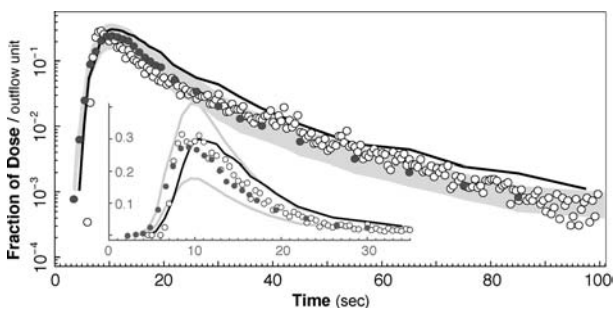

Fig. 7. Semilog and scatter plots show the fraction of dose per outflow unit (per ml for the referent) as a function of time (1 unit = 1 s) after dosing. Each dose contained SUCROSE and/or ANTIPYRINE. The ISL and the experimental protocol are same as in Fig. 4; parameter values are listed in the Appendix. Open circles: outflow values for ANTIPYRINE. Gray circles: antipyrine data from one rat liver (fraction of dose/ml; from Ref. (2)); black line-segments connect the data for coadministered sucrose. The width of the light gray SM band assumes the same variance as in Fig. 4. Inset: ANTIPYRINE coadministered with SUCROSE. The ANTIPYRINE data are smoothed, pooled results for 48 independent runs of the same ISL.

components), 7 (components easily *reconfigured* to represent different conditions), and 8 (simple to change assumptions or details without requiring significant re-engineering).

The first set of experiments (designated N) study sinusoidal network arrangement, and reference a control ISL, N1, which gave a good match to a referent sucrose outflow profile, similar to that presented in Fig. 4. The experimental group examined four changes, N2–N5: the zonal distribution of nodes is changed in four ways, as listed in Table 1, while all other parameter values are unaltered. In N2, the Zone I:II node ratio is changed from 30:15 to 25:20. In N3, the nodes are evenly distributed across all Zones. N4 is analogous to a retrograde perfusion in that nodes per zone are reversed relative to N1, whereas in N5 all the nodes are in one zone. The results for SUCROSE are presented in Fig. 8. The results for ANTIPYRINE were very similar (as would be expected), and so are not shown.

The results of experiments N1–N3 are within the *in silico* experimental system variability. The right shift of the peak in N4, the simulated "retrograde perfusion," is an artifact of the model implementation: with

Table 1. Values of primary parameters changed[a] in the network arrangement (*N*) and spatial relationships (*S*) experiments

Parameter	Experiment								
Nodes	N1	N2	N3	N4	N5	S1	S2	S3	S4
Zone									
I	30	25	16	2	0	30	30	30	30
II	15	20	16	15	47	20	20	20	20
III	2	2	15	30	0	3	3	3	3
Inter-zone connections									
I → II	15	20	16	15	0	20	20	20	20
II → III	2	2	15	30	0	10	10	10	10
Intra-zone connections									
I → I	15	12	8	1	0	20	0	20	20
II → II	7	10	8	7	23	15	15	15	15
$\boldsymbol{S}_A$ (% total)	80	80	80	80	80	90	90	90[b]	10
$\boldsymbol{S}_B$ (% total)	20	20	20	20	20	10	10	10[b]	90
Cell density, Grid B	0.8	0.8	0.8	0.8	0.8	0.95	0.95	0.95	0.95
Cell density, Grid C	0.2	0.2	0.2	0.2	0.2	0.95	0.95	0.95	0.95
Turbo	0.3	0.3	0.3	0.3	0.3	0.1	0.1	0.1	0.1

[a] The *N* experiments use 25 simulation runs; the *S* use 50. In all cases, there are no I → III and III → III connections. All other parameters are the same as for the sucrose outflow profile in Fig. 4.

[b] In S3 the surface-to-volume ratios of $\boldsymbol{S}_A$ and $\boldsymbol{S}_B$ are reversed; relative to $\boldsymbol{S}_B$ the $\boldsymbol{S}_A$ in this study have a shorter path length and a larger (rather than smaller) surface-to-volume ratio.

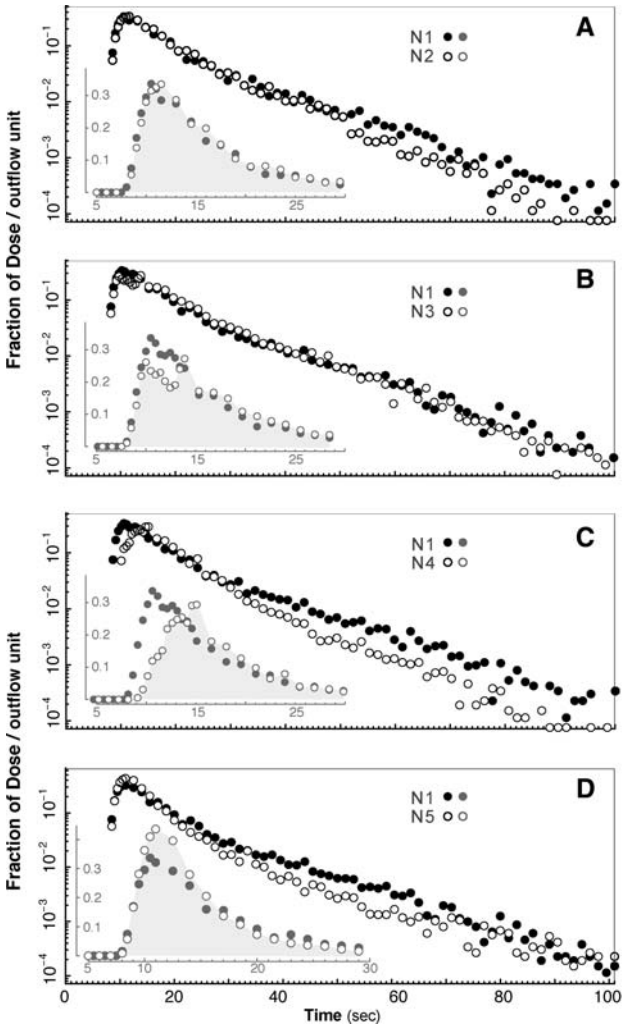

Fig. 8. Semilog and scatter plots, as in Fig. 4, of outflow fraction following dose administration to ISLs having different sinusoidal network arrangements. Each dose contained equal amounts of SUCROSE and ANTIPYRINE; only SUCROSE data are shown because the patterns for each were essentially the same. The outflow profiles were generated from ISLs with a control (N1; closed circles) and one of the four experimental arrangements (N2–N5; open circles) specified in Table 1. All other parameter values were unchanged relative to those of N1.

only two nodes in Zone I, there is insufficient space for the incoming dose, and so for a short interval it backs up at the PV source. The slightly higher peak for N5 relative to N1 is because there are more 1-node paths between PV and CV. The lower values between $t = 30$ and 70 followed by a somewhat shallower tail are a consequence of the random assignment of edges within this arrangement, allowing for more and longer multi-node paths. The data for N2–N4 provide a measure by which topological properties of the sinusoidal network can be prioritized, which would not be possible in a model induced solely from outflow profiles. The N5 results, supported by those from N2–N4, clearly demonstrate that in order to match antipyrine and sucrose profiles it is not necessary to have a three-zone arrangement. Rather, it is essential to have a sufficient number of inter-SS connections to insure a diversity of PV-to-CV path lengths.

The properties associated with zonation are expected to become more important for high clearance compounds. Relative to N1, it seems less likely that the SSs and the connections between them for N2–N5 could be arranged, three-dimensionally, in a biologically realistic way. Having structures that can be separately arranged in a biologically realistic way within a realistic 3D space was not one of our initially targeted attributes. When required, such requirements can be added easily because of the synthetic nature of the model. The N2–N5 structures are from outside that circumscribed space and so are invalid for normal livers (but possibly not for diseased livers).

The second set of experiments (designated S) explored the consequences of changes in relative spatial relationships within the ISL, starting with a parameterization (experiment S1) that gave a good match to a referent sucrose outflow profile (similar but not identical to N1). In S2, we eliminate all intra-zone cross-connections in Zone I. In S3, we reversed the $\boldsymbol{S}_A$ and $\boldsymbol{S}_B$ surface-to-volume ratios so that relative to $\boldsymbol{S}_B$ the $\boldsymbol{S}_A$ had a longer path length and a larger (rather than smaller) surface-to-volume ratio. In the last experiment (S4), we reversed the ratio of $\boldsymbol{S}_A$ to $\boldsymbol{S}_B$ SSs from 9:1 to 1:9. The results for SUCROSE are presented in Fig. 9. As with the experiments above, the results for ANTIPYRINE were very similar to those for SUCROSE, and so were not shown.

In S2, eliminating Zone I intra-connections resulted in an increase in the number of short PV-to-CV paths as evidenced by the slightly earlier and larger peak fraction. Changing SS spatial properties in S3 resulted in a considerable increase in space outside the Core. SUCROSE and ANTIPYRINE roamed around within this space, resulting in a lower peak fraction occurring later. It also caused a dramatic increase in the variance of the outflow data, because of the increased variation in length, volume, and area of all possible paths. Reversing the $\boldsymbol{S}_A$:$\boldsymbol{S}_B$ ratio (S4) also

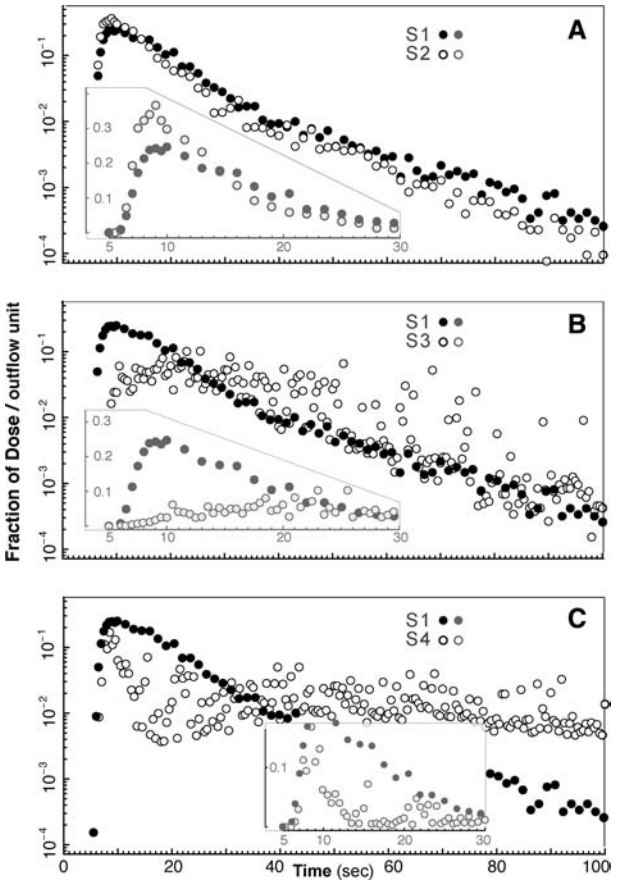

Fig. 9. Semilog and scatter plots, as in Fig. 4, show ISL outflow fraction following dose administration to ISLs having altered SS spatial relationships (*S*). Each dose contained equal amounts of SUCROSE and ANTIPYRINE; only SUCROSE data are shown because the patterns for each were essentially the same. The outflow profiles correspond to one of the four relationships detailed in the text; the parameterizations for S1, S2, and S4 are detailed in Table 1. (A) Relative to S1, for S2 all intra-zone connections in Zone 1 were eliminated. (B) Relative to S1, S3 had volume ratios of $\boldsymbol{S}_A$ and $\boldsymbol{S}_B$ that were reversed relative to S1. (C) Relative to S1, in S4 the $\boldsymbol{S}_A$ and $\boldsymbol{S}_B$ ratio was changed from 8:2 to 2:8. Otherwise, parameterizations were the same as for N1 and Fig. 4.

increases space outside the Core. This reversal apparently caused paths to form three clusters in terms of their properties, as evidenced by the three peaks in the outflow profile (at about $t = 8$, 22 and 40). The first peak is the result of a set of short, small capacity paths. Such variation in path properties may be characteristics of some hepatic disease states that

increase intrahepatic heterogeneity. These experiments support the extension of the convection-dispersion model to two compartments (9) while simultaneously providing for many more compartments to facilitate validation against observables with a finer-grain (higher information content) than the outflow profile.

DISCUSSION

The ISL is a representative of an entirely new class of physiologically based models. By designing components and composing them in a synthetic model capable of exhibiting nine of the ten targeted capabilities (discussed below) we have created a vehicle for continual clarification at multiple levels of what occurs within the liver during passage of compounds of interest. The greater the similarity between the properties and characteristics of the ISL and the liver attributes to which they map, the more useful the ISL is expected to become as a PBPK tool. We can make progress in achieving the larger PBPK vision by systematically increasing liver and ISL similarity at four levels:

- outflow or PK profiles;
- measures of related phenotypic attributes;
- generative components;
- component interactions and their organization.

Nine of Ten Capabilities Achieved and Demonstrated

Intrahepatic events. The fixed and dynamic relationships within the ISL (Figs. 1 and 2) are relativistic and realistic at the current level of resolution. For the specific, simple task of representing sucrose and antipyrine outflow profiles, components that are more accurate and detailed than those used proved not to be needed. Instead, it was important that component interactions *in silico* reasonably matched the corresponding referent interactions, such as the fraction of time ANTIPYRINE objects spend in different environments.

Physiological mapping. By conceptually extending the ISL model and the *in silico* experimental procedure beyond the liver to include key components associated with the actual wet-lab system, catheters and fraction collection, for example, it proved easier to make the observables from each consistent. It has been widely recognized that such system factors, outside of the biological component, must be factored into hepatic clearance mod-

els (35). The dosing function can be easily changed to represent different experimental systems without having to change any LOBULE property.

Two classes of observables influenced physiological mappings: histological and dynamic. We used the former to set constraints: acceptable *in silico* components and relationships needed to fall within those constraints to be consistent. Where they fell, such as the number of graph nodes, their interconnections and SS properties, and number of ENZYMES per HEPATOCYTE, were controlled by the dynamic observable, of which we had one type: outflow profiles. By increasing the number of compounds that an ISL can represent (discussed below), we will be iteratively improving the physiological mapping along with the accuracy of the detail within.

Turing test. Because of the many Monte Carlo controlled options at each cycle, each trek of dose through the same lobule is unique and no two lobules are identical. By pooling results from several simulations, we generated a unique outflow profile. In these ways, the ISL has represented uncertainty in observations as well as in the biology and the outflow profiles. Using an acceptably parameterized ISL, we demonstrated that once the SM criteria were satisfied, then from data alone, the results from wet-lab and *in silico* experiments were experimentally indistinguishable.

Transparency. The transparency of synthetic models helps bring conceptual clarity to the opacity of biological systems. We can record where SUCROSE and ANTIPYRINE go and what they do. We can then visualize such detail as the simulation progresses. We can, for example observe how any SS is connected to others or how many HEPATOCYTES an ANTIPYRINE visits before being METABOLIZED. From a modeling perspective, such capabilities provide a means of identifying potential flaws in the software, its assembly, and operation in ways that can feed back and influence the design of future experiments and how we think about the referent. Having transparency makes it possible to contrast visual and abstract features of the ISL and to observe how processes give rise to characteristic features. We can trace cause-effect relationships to specific subcellular components.

Articulation. To make model evolution facile, the PBPK modeler needs the ability to easily explore an alternate sinusoidal topography, for example, or to alter the spatial arrangement of TRANSPORTERS and ENZYMES (26,27). We have demonstrated that it is straightforward to plug SS components together, later disconnect them, and replace some with new components (Figs. 8 and 9). The same can be done within the SS functional unit: a grid or cells can be removed and modified. Cells can be added to or removed. The functions and interrelations of the other components remain unaltered.

Reconfigurability. Internal and external factors can lead to important differences between livers. The PBPK vision anticipates being able to explore the significance and consequences of such differences. Using directed graphs to represent connectivity between units of function, one of several possible approaches, enables us to manipulate the representation of both histology and physiology. We have shown that it is easy to alter these representations and explore the consequences. Although not demonstrated here, it is similarly easy to alter the experimental context. The ISL represents an isolated, perfused liver. By altering the lobule input functions, we can change the system to represent the liver in a living rat or within a different perfusion system. We can unplug HEPATOCYTES from the ISL and study their properties in simulated *in vitro* experimental conditions (28,29). Given appropriate *in vitro* data we can also refine, reparameterize and validate the HEPATOCYTES, and return them to the ISL to observe the consequences within the whole-liver context.

Change usage. With traditional PBPK models, changing assumptions as we did for Fig. 8, can require a different set of differential equations where the mapping between the new and the original parameters is not straightforward. This reality often hampers exploring the consequences of alternative sets of assumptions. Consequently, some PBPK models can acquire a degree of inertia. Researchers find it easier or more cost effective to adjust their requirements and model use to available models, thereby avoiding dealing with such challenges and forgoing the benefits they might have obtained. Elimination of such situations is the motivation for capability eight.

Multiple compounds. We have demonstrated a powerful, scientifically useful characteristic of the ISL. An ISL parameterized for one COMPOUND, SUCROSE in this case, can be used to represent the outflow profile of a new compound, such as ANTIPYRINE, without compromising the model's ability to interact as before with the first compound. We need only change those parameters that are influenced differently by the new compound's physicochemical properties. Should one or two new features be needed, they can be added without compromising existing ISL capabilities. It remains to be demonstrated if a single ISL can be extended to a large set of compounds. The ISL exists and is capable of functioning whether or not it is dosed with SUCROSE and/or ANTIPYRINE. Each COMPOUND has properties that can be recognized by the ISL components. They can even be given recognition algorithms so that after acquiring a mobile object's properties, the ISL components automatically adjust their responses according to a separate or learned algorithm and the objects they encounter.

Discrete interactions. We demonstrated that adopting graphs (networks) as a fundamental modeling tool allows us to achieve the above

nine capabilities. By restricting the model to discrete interactions, it ensures that graphs can be used throughout the ISL, which ensures the above nine capabilities and makes the resulting device more explorable.

Whole organism. Having the ISL become a component in a whole organism model is a special case of the *articulation*, *reconfigurability*, *and change usage* capabilities. Attaining it is essential to achieve the full PBPK vision and strengthen the case being made for this class of models. Aspects of an ISL can be separately validated against *in vitro* data, for example, prior to inclusion within the whole organism model.

Detail, Accuracy, and Realism

How much detail does an ISL need; how accurate and realistic does it need to be? The answers require having other information, such as a clear statement of why the model is needed. The PBPK vision is such a statement. We also need to state the uses to which the model will be put, such as to mimic specific aspects of hepatic functionality along with PCs of the referent system that we deem important for the analogue to possess. These PCs were a significant determinant of the detail reflected in Figs. 1 and 2. Depending on how PCs are specified, they will circumscribe a space of allowable ISLs that can range from relatively simple to complex. The referent PCs are expected to have direct counterparts in the ISLs. For example, if at least 50% of the sinusoids near the PV in the referent lobules are (or are assumed to be) interconnected, and this property is among the listed PCs, then at least 50% of the SSs near the PV in the ISL should be interconnected.

Most important are the measurable observables of the referent. They are used for model validation (see Supplementary Material). They circumscribe the behavior space of each ISL. The similarity measures used to compare referent and ISL observables provide an acceptance criterion for the accuracy; and so, indirectly they are part of the ISL specification. They influence the ISL's detail and fidelity. For example, if we had decided to be satisfied with outflow profiles that fit within a ±2SD band about the target outflow data, and we had decided to tolerate a few modest bumps in the simulated outflow profile, then we could have accepted lobule graph structures having significantly less detail.

Several ISL features can be cited as being realistic; others can be criticized as being unrealistic. We have dealt with the former. Relative to the latter, here are three examples. (1) In a lobule, only adjacent sinusoids are interconnected, whereas in the ISL, connections between nodes are randomly assigned without consideration of relative location. (2) Because the $\boldsymbol{S}_A$ and $\boldsymbol{S}_B$ are randomly assigned, the range of path lengths in terms

of total grid length can be unrealistically broad. For example a one-node path could be as short as two grid spaces in length; whereas, a three-node path could be 50 grid spaces or longer. It seems unlikely that the range in actual lobule path lengths will be that broad. To make relative path lengths more realistic, we need to add a data-driven constraint to our list of targeted PCs. (3) The graph structures (Fig. 6) are intended to represent plausible *paths*, not actual measurable lengths. They are not intended to be scale models of actual sinusoidal arrangements.

Because of the random assignment of edges, a Zone 1 or 2 node can be connected to itself by a single edge (the loop in graphs 002 and 010 in Fig. 6) that forces some compound to revisit the same region of functionality many times. We did not eliminate this feature because, even though it does not seem realistic, we did not have experimental evidence to rule out such path options occurring at a low frequency. Should the evidence become available (or a convincing argument be offered) that no such paths exist in livers, a constraint can be added disallowing them.

The ISL is complicated, and yet we are only dealing with antipyrine and sucrose. We do not yet address any of the potentially complex intracellular events encountered by some drugs. Is this ISL too complicated? To achieve the PBPK vision will require a combination of sophisticated knowledge, skills, and tools. The problems can have complex origins. Complicated problem solving and decision-making skills require complicated technology (or experienced experts or both). As the overlap between *in silico* and referent phenotypes increases, the complexity of ISLs and similar devices will approach that of their referents.

CONCLUSION

There is increasing impetus for the inclusion of *in silico* PBPK modeling in defining compound PK properties and their suitability for clinical use (36). To achieve these goals it is becoming necessary to provide increasingly more useful predictions and detailed explanations for observed PK behaviors and properties. Achieving the required detail is limited by the abstractive nature and inherent heuristic limitations of current inductive PBPK models. The synthetic ISL is an early example of a class of models specifically intended to help provide the required detail and deliver improved insights.

APPENDIX

Table A1. Description of ISL Parameters and Their Values for the Simulations in Figs. 4 and 5

Parameter[a]	Description	Value(s) S/(S+A)[b]	Range[c]
Device framework parameters			
cycleLimit	(B)[d] Provides the simulation with an artificial stopping criterion so that it will not run forever.	200	200
monteCarloRuns	(I)[d] The number of runs in a Monte-Carlo set. Aggregate measures for the whole system are calculated at the end of all Monte-Carlo runs.	48	[2, 50]
similarityMeasure	Specifies which similarity measure to use.	global_sd	global_sd
nominalProfile	(S)[d] Specifies which model to use as the nominal for use in calculating similarity between the experimental and nominal models.		
experimentalProfile	(S) Specifies which model to use as the experimental for use in calculating similarity between the experimental and nominal models.		
In silico liver parameters			
StepsPerCycle	(I) Parametrizes the granularity of time for the Research model (the ISL). The data have a "sampling rate" that provides a default time scale for it. Finer granularity requires interpolation between the data points. The Reference (PK) model[a] is a time-reversible, continuous function, which allows sampling at any frequency.	2	2
GraphInputFile	(S) Specifies the file to read if the SS graph is to be specified by an explicit graph (file format is GML). (S) Provides the lobule graphical specification, and specifies the base file name (extension.ls) to be used if the graph is to be specified according to the Lobule Specification.	null	
	Nodes in Zone I	30	[20, 30]
	Nodes in Zone II	20	[10, 30]
	Nodes in Zone III	3	[3, 15]
GraphSpecFile			
	Intra-Zone I edges	20/13	[10, 30]
	Intra-Zone II edges	15/9	[5, 25]

Table A1. Continued

	Intra-Zone III edges	0	0
	Zone I → Zone II edges	20/25	[2, 45]
	Zone I → Zone III edges	0	[1, 20]
	Zone II → Zone III edges	10/15	[5, 25]
GraphSpecIterates	(I) Tells the framework to modify LOBULE specification and run a Monte-Carlo set (consisting of N runs) for each different LOBULE specification. Set to 1, it runs 1 set and provides 1 set of outputs. Set to 5, the first run uses the current contents of lobule.ls; it then runs 4 more sets, slightly modifying the LOBULE specification each time, resulting in 5 sets.	1	[1, 10]
DirSinRatio	(F)[d] Specifies the percentage of SS that are type $\boldsymbol{S}_A$ ("direct").	0.90/0.875	[0, 1]
TortSinRatio	(F) Specifies the percentage of SS that are $\boldsymbol{S}_B$ ("tortuous").	0.10/0.125	[0, 1]
DirSinCircMin	(I) Sets the upper and lower bounds for a pseudo-RNG (random number generator) using the uniform distribution to choose a circumference for each SS.	50	[1, 50]
DirSinCircMax		50	[1, 100]
TortSinCircMin		4	[1, 4]
TortSinCircMax		4	[1, 20]
DirSinLenAlpha	(F) Sets the parameters for a pseudo-RNG using a modified form of the Gamma distribution; the modification consists of a left-right shift of the distribution, allowing the user to clip off the front.	2.0	[0.5, 3.0]
DirSinLenBeta		0.215	[0.125, 0.325]
DirSinLenShift		0.0	0.0
TortSinLenAlpha		10.0	[6, 18]
TortSinLenBeta		0.10/0.1125	[0.03, 0.14]
TortSinLenShift		−35.0/−32.5	−(40.0, −35.0)
SinusoidTurbo	(F) The complement of the amount of turbulence allowed in any given SS. Lower turbo means more tendency of any one COMPOUND to wander sideways or backwards. Higher Turbo means a stronger flow from the input to the output of the SS.	0.1/0.2	[0.05, 0.95]

Table A1. Continued

ECDensity	(F) Specifies the relative ENDOTHELIAL CELL density, given that the number of grid points in Grid B is set by the geometry parameters of the SS; it specifies the percentage of Grid B points that index an endothelial cell.	0.95	[0.25, 1.00]
ECDensity	(F) Specifies the relative ENDOTHELIAL CELL density, given that the number of grid points in Grid B is set by the geometry parameters of the SS; it specifies the percentage of Grid B points that index an endothelial cell.	0.95	[0.25, 1.00]
HepDensity	(F) Specifies the relative HEPATOCYTES density within Grid C, given that the number of grid points in Grid C is set by the geometry parameters of the SS, it specifies the percentage of Grid C points that index a hepatocyte.	0.95	[0.15, 0.99]
CoreFlowRate	(I) The number of slots solute in the SS core moves forward during each step.	3	[1, 5]
S2EJumpProb	(F) Specifies the probability that, when given the option, SUCROSE will jump from the sinusoid rim space to the endothelial space.	0.5/0.35	–
E2SJumpProb	(F) Specifies the probability that, when given the option, SUCROSE will jump from the endothelial space to the sinusoid rim space.	0.5	–
E2DJumpProb	(F) Specifies the probability that, when given the option, SUCROSE will jump from the endothelial space to the space of dissé.	0.5/0.35	–
D2EJumpProb	(F) Specifies the probability that, when given the option, SUCROSE will jump from the space of dissé to the endothelial space.	0.5	–

Table A1. Continued

BindersPerCellMin	(I) Max and min for a uniform pseudo-random draw for the number of binding agents inside each CELL. Simple binders for ECs and ENZYMES for HEPATOCYTES.	5	
BindersPerCellMax		37	
MetabolizationProb	(F) Probability that an ENZYME will metabolize a SOLUTE before it releases it.	0.10	[0, 1]
SoluteBindingProb	(F) Probability that, when a binder and SOLUTE make contact, the SOLUTE will be bound.	0.15	[0, 1]
SoluteBindingCycles	(I) Number of cycles a binder will bind a solute.	10	
SoluteScale	(F) Specifies the number of molecules being represented by one COMPOUND. Because everything in the model is normalized, this amounts to a magnitude factor on the output fraction.	7.0	[1.0, 8.0]
BolusStartTime	(I) Dictates when to let COMPOUNDS flow into the LOBULE.	5	[4, 7]
DosageParam[e]	(F) Parameter (A) of the dosage function: $D(t) = A[B^C t^{(C-1)} e^{(-Bt)}]/(C-1)!$, where t = current cycle; parameter (A) simply raises the amplitude of the function.	2000	[1000, 7000]
DosageParamB	(F) Parameter (B) of the dosage function.	1	[1, 2]
DosageParamC	(F) Parameter (C) of the dosage function.	2	[2, 3]
	Actual dose for Fig. 4.	3,682	

[a] There are four classes of parameters: device framework, research model, reference model, and data model. Here, the research model is the ISL. Only a subset of the device framework parameters is listed here. The data model includes all the data against which the SM is being applied, and uses a parameter that specifies whether to interpolate between observations of the *in silico* data. The reference model is a traditional PK model previously fit to the *in silico* experimental data; it is run concurrently with the research model.

[b] S: parameter values when only SUCROSE was dosed; $(S+A)$ parameter values when SUCROSE and ANTIPYRINE were dosed in combination.

[c] Ranges from which values were drawn during searches of model and parameter space.

[d] B: Boolean; F: floating; I: integer; S: string.

[e] The total dose is the area under the dosage function curve.

Table A2. A comparison of parameters values for the sucrose outflow profiles in Figs. 4 and 5A

Parameter	Fig. 4 value(s)	Fig. 5A value(s)
Nodes in Zone II	20	15
Nodes in Zone III	3	2
Intra-Zone edge: I	20	15
Intra-Zone edge: II	15	7
Intra-Zone edge: III	0	0
Edges		
Zone I → II	20	15
Zone I → III	0	0
Zone II → III	10	2
DirSinRatio	0.90	0.80
TortSinRatio	0.10	0.20
TortSinLenBeta	0.10	0.105
TortSinLenShift	−35.0	−40.0
SinusoidTurbo	0.1	0.3
ECDensity	0.95	0.8
HepDensity	0.95	0.4
S2EJumpProb	0.5	0.3
E2SJumpProb	0.5	0.3
E2DJumpProb	0.5	0.3
D2EJumpProb	0.5	0.3
BolusStartTime	5	4

[a] The parameters are the same as in Table A1. Only the parameters that are different between Figs. 4 and 5 are listed. All other parameter values are as listed in Table A1.

ACKNOWLEDGMENTS

For valuable technical assistance, we thank G. Cosmo Haun, and for theoretical, biological, and practical advice, we thank Bernie Zeigler, Betty Hoener, and Zbigniew Kmiec. This work is reflected in the content of Li Yan's Ph.D. dissertation. For their helpful advice and commentary on the manuscript, along with helpful discussions and suggestions, we thank Jesse Engelberg, Pearl Johnson, Sunwoo Park, Shahab Sheikh-Bahaei, Teddy Lam, Suman Ganguli, Sean Kim, Mark Grant, and other members of the BioSystems Group along with Tom Robertson and Narelle Walker from UQ. CAH thanks Amina Qutub for her early efforts in agent-based modeling. We are grateful for the financial support of the CDH Research Foundation (of which CAH is a trustee), the National Health and Medical Research Council of Australia, the Queensland and New South Wales Lions Medical Research Foundation, and CAH. We are especially grateful to the Swarm Development Group, Debian, and the Free Software

Foundation for making all the tools. Earlier versions of the ISL were presented and discussed at the Computational Methods in Systems Biology, Second International Workshop, CMSB 2004, (37), and at the 26th Annual International Conference of the Engineering in Medicine and Biology Society, September, 2004.

SUPPLEMENTARY MATERIAL

Visualizations of compounds moving within a SS and an entire LOBULE are available at [http://dx.doi.org/10.1007/s10928-006-9031-3]. The supplementary material includes additional detail on the following eight topics: (1) the inductive and synthetic methods; (2) contrasting inductive and synthetic models; (3) comparison of inductive and synthetic models; (4) validation of synthetic models; (5) *in silico* framework: technical detail; (6) *in silico* experimental method; (7) building an acceptable *in silico* liver model; and (8) higher and lower levels of resolution.

REFERENCES

1. M. Rowland. Physiologic pharmacokinetic models: relevance, experience, and future trends. *Drug Metab. Rev.* **15**:55–74 (1984).
2. D. Y. Hung, P. Chang, M. Weiss, and M. S. Roberts. Structure-hepatic disposition relationships for cationic drugs in isolated perfused rat livers: transmembrane exchange and cytoplasmic binding process. *J. Pharmacol. Exper. Therap.* **297**:780–89 (2001).
3. J. B. Bassingthwaite. Blood flow and diffusion through mammalian organs. *Science* **167**:1347–53 (1970).
4. M. Rowland, L. Balant, and C. Peck. Physiologically based pharmacokinetics in drug development and regulatory science: a workshop report (Georgetown University, Washington, DC, May 29–30, 2002). *AAPS PharmSci.* **6**: article 6. DOI: 10.1208/ps060106 (2004).
5. M. E. Andersen. Toxicokinetic modeling and its applications in chemical risk assessment. *Toxicol. Lett.* **138**(1–2):9–27 (2003).
6. D. E. Leahy. Progress in simulation modelling for pharmacokinetics. *Curr. Top. Med. Chem.* **3**:1257–68 (2003).
7. R. A. Corley, T. J. Mast, E. W. Carney, J. M. Rogers, and G. P. Daston. Evaluation of physiologically based models of pregnancy and lactation for their application in children's health risk assessments. *Crit. Rev. Toxicol.* **34**(2):137–211 (2003).
8. M. S. Roberts, B. M. Magnusson, F. J. Burczynski, and M. Weiss. Enterohepatic circulation: physiological, pharmacokinetic and clinical implications. *Clin. Pharmacokinet.* **41**:751–90 (2002).
9. M. S. Roberts and Y. G. Anissimov. Modeling of hepatic elimination and organ distribution kinetics with the extended convection-dispersion model. *J. Pharmacokin. Biopharm.* **27**:343–382 (1999).
10. B. P. Zeigler, H. Praehofer, and T. G. Kim. *Theory of Modeling and Simulation: Integrating Discrete Event and Continuous Complex Dynamic Systems*. Academic Press, California, 2000, pp. 3–36, 75–85, 99–104, 137–147.
11. L. Steels and R. Brooks (eds.). *The Artificial Life Route to Artificial Intelligence*. Lawrence Earlbaum Associates Inc., New Jersey, 1995, pp. 83–121.

12. K. Czarnecki and U. Eisenecker. *Generative Programming: Methods, Tools, and Applications*. Addison-Wesley, New York, 2000, pp. 10, 251–254.
13. G. E. Ropella, C. A. Hunt, and D. A. Nag. Using heuristic models to bridge the gap between analytic and experimental models in biology. *2005 Spring Simulation Multiconference*, The Society for Modeling and Simulation International, San Diego, CA, April 2–8, 2005.
14. G. E. Ropella, C. A. Hunt, and S. Sheikh-Bahaei. Methodological considerations of heuristic modeling of biological systems. *The 9th World Multi-Conference on Systemics, Cybernetics and Informatics*, Orlando, FL, July 10–13, 2005.
15. D.E. Leahy. Progress in simulation modelling for pharmacokinetics. *Curr. Top. Med. Chem.* **3**(11):1257–1268 (2003).
16. H. F. Teutsch, D. Schuerfeld, and E. Groezinger. Three-dimensional reconstruction of parenchymal units in the liver of the rat. *Hepatology* **29**:494–505 (1999).
17. S.M. Peirce, E.J. van Gieson, and T.C. Skalak. Multicellular simulation predicts microvascular patterning and in silico tissue assembly. *FASEB J.* **18**:731–33 (2004).
18. G. An. *In-silico* experiments of existing and hypothetical cytokine-directed clinical trials using agent based modeling. *Crit. Care Med.* **32**:2050–2060 (2004).
19. J. J. Gumucio and D. L. Miller. Zonal hepatic function: solute-hepatocyte interactions within the liver acinus. *Prog. Liver. Diseases.* **7**:17–30 (1982).
20. Y. Kato, J. Tanaka, and K. Koyama. Intralobular heterogeneity of oxidative stress and cell death in ischemia-reperfused rat liver. *J. Surg. Res.* **95**:99–106 (2001).
21. J. Y. Scoazec, L. Racine, A. Couvelard, J. F. Flejou, and G. Geldmann. Endothelial cell heterogeneity in the normal human liver acinus: *in silico* immunohistochemical demonstration. *Liver* **14**:113–23 (1994).
22. R. S. McCuskey. Morphological mechanisms for regulating blood flow through hepatic sinusoids. *Liver* **20**:3–7 (2000).
23. A. Koo, I. Y. Liang, and K. K. Cheng. The terminal hepatic microcirculation in the rat. *Quart. J. Exp. Physiol. Cogn. Med.* **60**:261–266 (1975).
24. D. L. Miller, C. S. Zanolli, and J. J. Gumucio. Quantitative morphology of the sinusoids of the hepatic acinus. *Gastroenterology* **76**:965–969 (1979).
25. K. Cheung, P. E. Hickman, J. M. Potter, N. Walker, M. Jericho, R. Haslam, and M. S. Roberts. An optimised model for rat liver perfusion studies. *J. Surg. Res.* **66**:81–89 (1996).
26. Y. Liu and C. A. Hunt. Studies of intestinal drug transport using an in silico epithelio-mimetic device. *Biosystems* **82**(2):154–167 (2005).
27. Y. Liu and C. A. Hunt. Mechanistic study of the interplay of intestinal transport and metabolism using the synthetic modeling method. *Pharm. Res.* **23**(3):493–505 (2006).
28. S. Sheikh-Bahaei, G. E. P. Ropella, and C. A. Hunt. Agent-based simulation of in vitro hepatic drug metabolism: *in silico* hepatic intrinsic clearance. *2005 Spring Simulation Multiconference*, The Society for Modeling and Simulation International, San Diego, CA, April 2–8, 2005.
29. S. Sheikh-Bahaei, G. E. P. Ropella, and C. A. Hunt. *In silico* hepatocyte: agent-based modeling of the biliary excretion of drugs. *2006 Spring Simulation Multiconference*, The Society for Modeling and Simulation International, Huntsville, AL, April 2–6, 2006.
30. S. Santini and R. Jain. Similarity Measures. *IEEE Trans. Pattern Anal. Mach. Intell.* **21**(9):871–83 (1999).
31. D. A. Nag, G. E. P. Ropella, and C. A. Hunt. Similarity measures and validation in automated modeling. *Huntsville Simulation Conference*, Huntsville, AL, October 25–27, 2005.
32. C. A. Goresky. A linear method for determining liver sinusoidal and extravascular volumes. *Am. J. Physiol.* 204:626–40 (1963).
33. K. S. Pang, W.-F. Lee, W. F. Cherry, V. Yuen, J. Accaputo, S. Fayz, A. J. Schwab, and C. A. Goresky. Effects of perfusate flow rate on measured blood volume, Disse space, intracellular water space, and drug extraction in the perfused rat liver preparation: characterization by the multiple indicator dilution technique. *J. Pharmacokinet. Biopharm.* **16**:595–632 (1988).

34. A. J. Schwab and K. S. Pang. The multiple indicator-dilution method for the study of enzyme heterogeneity in liver: theoretical basis. *Drug Metab. Dispos.* **27**:746–55 (1999).
35. Y. G. Anissimov, A. J. Bracken, and M. S. Roberts. Catheter effects in organ perfusion experiments. *J. Theor. Biol.* **214**:263–73 (2002).
36. Food and Drug Administration. *Innovation or Stagnation: Challenge and Opportunity on the Critical Path to New Medical Products* [online], <http://www.fda.gov/oc/initiatives/criticalpath/whitepaper.html> (2004).
37. C. A. Hunt, G. E.P. Ropella, M. S. Roberts, and L. Yan. Biomimetic *in silico* devices. *Lecture Notes in Bioinformatics* **3082**:35–43 (2005).